Global estimates of dry ammonia deposition inferred from space-measurements

Lei Liu [a,*], Xiuying Zhang [b,*], Wen Xu [c], Xuejun Liu [c], Jing Wei [d,e], Zhen Wang [b], Yuyu Yang [a]

[a] College of Earth and Environmental Sciences, Lanzhou University, Lanzhou 730000, China
[b] International Institute for Earth System Science, Nanjing University, Nanjing 210023, China
[c] College of Resources and Environmental Sciences, National Academy of Agriculture Green Development, China Agricultural University, Beijing 100193, China
[d] State Key Laboratory of Remote Sensing Science, College of Global Change and Earth System Science, Beijing Normal University, Beijing, China
[e] Department of Atmospheric and Oceanic Science, Earth System Science Interdisciplinary Center, University of Maryland, College Park, MD, USA

HIGHLIGHTS

- A new satellite-based method is proposed to estimate dry ammonia deposition.
- An overestimation in dry ammonia deposition will be caused using unidirectional methods.
- Satellite-based estimates capture the general variability of dry ammonia deposition.

GRAPHICAL ABSTRACT
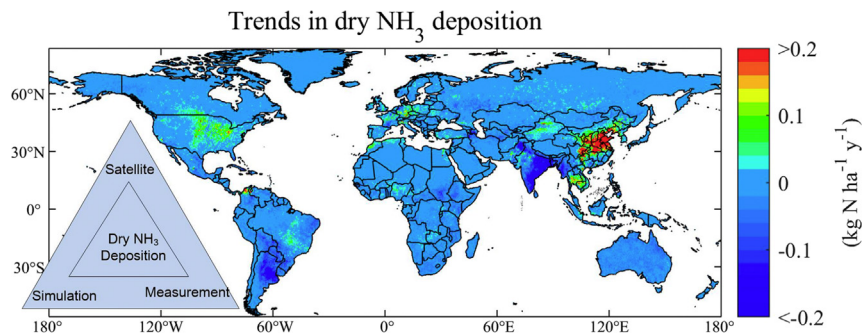
ARTICLE INFO

ABSTRACT

Ammonia (NH_3), as an alkaline gas, contributes substantially to atmospheric nitrogen deposition, which can cause biodiversity loss, water eutrophication and soil acidification. Advances in the application of satellite observations allow us to gain deeper insights into atmospheric NH_3 concentrations at large spatial scales. A new satellite-based methodology is proposed for estimating dry NH_3 deposition with consideration of bi-directional NH_3 exchange. We estimate the global dry NH_3 deposition for nine years (2008–2016) by using the Infrared Atmospheric Sounding Interferometer Instrument (IASI) NH_3 retrievals. Satellite-based dry NH_3 deposition is in general consistent with measured dry NH_3 deposition over the monitoring sites ($R^2 = 0.65$). Global dry NH_3 deposition over 8 kg N ha^{-1} is mainly distributed in the Eastern China, Northern and Central Pakistan, and Northern India. An annual increase rate of 0.27 and 0.13 kg N ha^{-1} y^{-1} in dry NH_3 deposition during 2008–2016 occurs in Eastern China and Sichuan Basin, which are the major Chinese agricultural regions. The NH_3 compensation point is high during warm months, and can be above 1 μg m^{-3} such as in Eastern China, implying the importance of considering the NH_3 compensation points for estimating dry NH_3 deposition. We find, if the upward NH_3 flux was ignored, it will cause 11%, 17%, 5% and 3% overestimation in dry NH_3 deposition in Eastern China, Northern India, Eastern United States and Western Europe, respectively. This study presents the potential of using the satellite retrievals to estimate the large-scale dry NH_3 deposition, and the methodology is able to provide temporally continuous and spatially complete fine-resolution datasets.

© 2018 Published by Elsevier B.V.

* Corresponding authors.
  E-mail addresses: liuleigeo@lzu.edu.cn (L. Liu), zhangxy@nju.edu.cn (X. Zhang).

1. Introduction

Global reactive nitrogen (N) increased greatly since the industrial revolution due to the dramatic growth of food and energy production (Galloway et al., 2008; Wei et al., 2019a). Ammonia (NH_3), as an alkaline gas, significantly contributes to neutralizing acids and then forming ammonium (NH_4^+) particulate matter (Yu et al., 2018; Zhang et al., 2013). Excessive atmospheric deposition of NH_3 and NH_4^+ can also cause damage to sensitive ecosystems (Endo et al., 2011). It is critical to quantify the global dry NH_3 deposition to evaluate its consequences to ecosystems and environment.

NH_3 exhibits bidirectional air-surface exchange including both upward and downward transportation (Ludwig et al., 2001; Sutton et al., 2013). Most previous works estimating large-scale dry NH_3 deposition considered only the deposition process and neglected the potential bidirectional exchange between the air and earth surface (Qi et al., 2013; Reay et al., 2008; Sickles II and Shadwick, 2015; Zhang et al., 2003). The phenomenon of air-surface NH_3 exchange was observed in numerous ground-based measurements (Azouz et al., 2019; Husted et al., 2010; Sutton et al., 2000; Sutton et al., 2010), suggesting the existence of a so-called "NH_3 compensation point" controlling dry NH_3 deposition. The NH_3 compensation point represents the combined effects of N availability, plant physiology and the complex soil processes (Sutton et al., 1994; Sutton et al., 1998). Bidirectional air-surface NH_3 exchange based on ground-based observations have been comprehensively reviewed by a previous study (Zhang et al., 2010), which provided valuable datasets on the stomatal and soil NH_3 emission potentials by different land use types. However, evaluation of large-scale dry NH_3 deposition is still difficult due to the sparse ground-based measurements around the globe (Jia et al., 2016; Nemitz et al., 2000).

Recent advances in the application of satellite NH_3 retrievals with large-scale spatial coverage (Van Damme et al., 2018; Warner et al., 2016) make it possible to evaluate global spatial and temporal atmospheric NH_3 abundance in more details. Global satellite NH_3 retrievals provide great potentials to estimate large-scale surface NH_3 concentrations and dry NH_3 deposition. Estimating global surface NH_3 concentrations is a prerequisite for estimating dry NH_3 deposition, when using bidirectional dry deposition scheme. A previous study used CrIS (Cross-track Infrared Sounder) NH_3 retrievals to estimate dry NH_3 deposition in North America, but ignoring the upward NH_3 fluxes (Kharol et al., 2018). Another study used the IASI (Infrared Atmospheric Sounding Interferometer) NH_3 retrievals to estimate the dry NH_3 deposition in Europe (Graaf et al., 2018), which only concerned the downward NH_3 process. Liu et al. (Liu et al., 2019) followed these studies, and gained the global surface NH_3 concentrations with a validation by ground-based measurements.

In this study, we use IASI NH_3 retrievals to estimate the global dry NH_3 deposition, with consideration of bi-directional air-surface exchange rather than the commonly used unidirectional dry deposition scheme, followed by a validation of the estimated dry NH_3 deposition with the ground-based measurements. We aim to explore a simple, fast and practical approach from a satellite perspective to gain an overall insight into spatiotemporal global dry NH_3 deposition, and assess the overall bi-directional NH_3 exchange over the globe.

2. Data

2.1. IASI NH_3 retrievals

As a passive satellite instrument, IASI (Infrared Atmospheric Sounding Interferometer Instrument) measures the infrared radiation in the spectral ranges of 645–2760 cm^{-1} from earth and atmosphere, operating in downward viewing geometry (Van Damme et al., 2014a). IASI NH_3 retrievals were gained from the Metop-A at 9:30 and 21:30 local time with spatial resolutions ranging from 12 × 12 km^2 to 20 × 39 km^2. Only measurements in the morning (at 9:30) were used in this study, since they are more sensitive to the atmospheric NH_3, linked with the thermal contrast (Van Damme et al., 2014b). We used the ANNI-NH3-v2.1R-I retrievals from 2008 to 2016 (Van Damme et al., 2017), which were based on an artificial neural network by converting a hyperspectral range index to NH_3 column (the driven data also included the meteorological data such as water vapour, pressure and temperature) (Van Damme et al., 2017; Whitburn et al., 2016). The ANNI-NH3-v2.1R-I can be used to analyze the inter-annual trends of atmosphere NH_3. There are no vertical profiles for each measurement in the ANNI-NH3-v2.1R-I. The retrievals with a relative error above 100% or an absolute error above 10^{16} molec cm^{-2} were excluded in this study. We processed the daily IASI NH_3 columns to the monthly average of the retrievals at 0.25° grids using arithmetic averaging methods, which were then used to estimate dry NH_3 deposition. Fig. S1 shows an example of spatial distributions of IASI NH_3 columns in 2014 using the arithmetic averaging methods. For more information on this dataset including the algorithm and the quality control, please refer to the previously published papers (Liu et al., 2019; Liu et al., 2017; Van Damme et al., 2017; Whitburn et al., 2016).

2.2. Surface NH_3 measurements

Dry NH_3 deposition is not measured directly from different regional networks including the Nationwide Nitrogen Deposition Monitoring Network (NNDMN) in China, the European Monitoring and Evaluation Programme (EMEP) and the Ammonia Monitoring Network (AMoN) in the US, because of the requirements for expensive instrumentation and complex methods. Instead, the surface NH_3 concentrations were measured directly, and then the dry NH_3 deposition can be obtained indirectly by combining the measured NH_3 concentrations with the modeled deposition velocity of NH_3 using the inferential methods. The measured surface NH_3 concentrations in NNDMN, AMoN-US and EMEP were used here to calculate the dry NH_3 deposition, combining the modeled deposition velocity. Then, dry NH_3 deposition at the monitoring sites was contrasted with the estimates. The NNDMN used DELTA and the ALPHA systems, and the AMoN-US used the radiello diffusive sampler, while the EMEP used the multiple measurement systems since it consists of multiple countries in Europe. The overall biases of the measurements were below 30% by different measurement systems from the networks (Bobrutzki et al., 2010; Sutton et al., 2001; Xu et al., 2015).

2.3. NH_3 vertical concentration

The GEOS-Chem, as a widely used atmospheric chemical transport model, was applied here to simulate NH_3 vertical profiles. GEOS-Chem is driven by the GEOS-FP meteorological data by NASA GMAO, and includes the simulation of NH_3-H_2SO_4-HNO_3 chemistry (Fountoukis and Nenes, 2007; Pye et al., 2009), adopted by the ISORROPIA II model. NH_3 emission inputs were obtained from EDGAR, with updates by regional datasets (such as MIX in Asian, EMEP in Europe and NEI in the US) (Chen et al., 2009; Kharol et al., 2018). Dry deposition of NH_3 follows the big-leaf models (Wang et al., 1998; Wesely, 1989), without considering the bidirectional NH_3 exchange. We here used the 47 layers' vertical NH_3 concentrations at 2° × 2.5° grids to construct the NH_3 vertical profile models.

3. Methodology

We firstly presented a brief description of procedures applied to estimate dry NH_3 deposition, and then gave detailed information for the satellite-based methods.

3.1. Method steps

The general flowchart of using satellite data to estimate dry NH_3 deposition with a module of air-surface exchange of NH_3 is shown in Fig. 1. IASI NH_3 retrievals are column data that have no vertical profiles. We gained surface NH_3 concentration by using modeled NH_3 vertical profiles. We constructed the Gaussian model to fit the 47 layers' vertical NH_3 concentrations, which can generate the continuous NH_3 profile. Hence, based on the constructed the Gaussian model, we can obtain satellite-based NH_3 concentration at any height. More importantly, the constructed the Gaussian model has general rules, appropriate for converting satellite columns to surface concentration simply. We have the following major steps:

Step 1: Construct the NH_3 vertical profiles. We try to generate NH_3 vertical profile models that can be applied to convert IASI NH_3 columns to surface NH_3 estimates quickly and simply. The widely used GEOS-Chem outputs including 47 layers' NH_3 concentrations from the surface to the troposphere are the best available datasets that can be used to construct the NH_3 vertical profile models.

Step 2: Estimate surface NH_3 concentration by IASI at fine resolutions. With the constructed vertical profiles (step 1), we can estimate the ratio of surface NH_3 concentrations (at any height) to total columns, and then use this ratio and IASI NH_3 columns to gain the satellite-based surface NH_3 estimates at fine resolutions (0.25° grids in this study).

Step 3: Estimate the NH_3 emission potentials. The NH_4^+ and H^+ in the soil are important variables to determine the soil NH_3 emission potentials. We try to model the NH_4^+ and H^+ in the soil with consideration of the N fertilization using the processed model DNDC (See the Sect. 1.1 in the supporting information). The stomatal NH_3 emission potentials were calculated by combining the LAI and the ratio of NH_4^+ and H^+ in the apoplastic fluid based on ground-based measurements in different land use types.

Step 4: Estimate canopy NH_3 compensation points. Stomatal and soil compensation points are then estimated by the estimated stomatal and soil NH_3 emission potentials. Then, calculate the NH_3 compensation points combining both the stomatal and soil compensation points.

Step 5: Estimate the deposition velocity of NH_3. The deposition velocity of NH_3 is related to aerodynamic resistance and quasi-

laminar sub-layer resistance, which can be estimated using the meteorological data under different land use types.

Step 6: Estimate the dry deposition of NH_3. Combined with the satellite-derived surface NH_3 concentrations, NH_3 compensation points and its deposition velocity, the dry NH_3 deposition can be estimated using the widely used inferential methods.

3.2. Estimating dry NH_3 deposition with Bi-directional air-surface exchange models

NH_3 can be volatilized from the ground to the atmosphere, and can also be deposited back to the ground, which is called bidirectional flux (Sutton et al., 2013; Zhang et al., 2010). The fundamental concept to estimate dry NH_3 deposition is based on the bi-directional air-surface exchange models (Nemitz et al., 2001; Sutton et al., 1998), which can be expressed by (Zhang et al., 2010):

$$F = (C - C_0) \times V_d \tag{1}$$

$$V_d = \frac{1}{R_a + R_b} \tag{2}$$

where C and C_0 are the surface NH_3 concentrations ($\mu g\ m^{-3}$) and the NH_3 compensation points; V_d is the deposition velocity ($cm\ s^{-1}$); R_a and R_b are aerodynamic resistance and quasi-laminar sub-layer resistance. R_a and R_b can be calculated by (Erisman et al., 1994):

$$R_a(z) = \frac{1}{ku} \left[\ln\frac{z-d}{z_0} - \varphi_h\left(\frac{z-d}{L}\right) + \varphi_h\left(\frac{z_0}{L}\right) \right] \tag{3}$$

$$R_b = \frac{2}{ku} \left(\frac{Sc}{Pr}\right)^{2/3} \tag{4}$$

where k indicates the Von Karman constant (0.4); u indicates the friction velocity; Z_0 represents the roughness length and L represents the Monin-Obukhov length; φ_h represents the stability function for heat; Pr and Sc are the Prandtl and Schmidt numbers.

Surface NH_3 concentration can be estimated by combining IASI-derived NH_3 columns and the NH_3 vertical profiles. The NH_3 vertical profiles can be well fitted by a Gaussian function based on 47 layers' NH_3 concentrations from the GEOS-Chem outputs (Liu et al., 2019). Based on the function of NH_3 vertical profiles and IASI NH_3 columns,
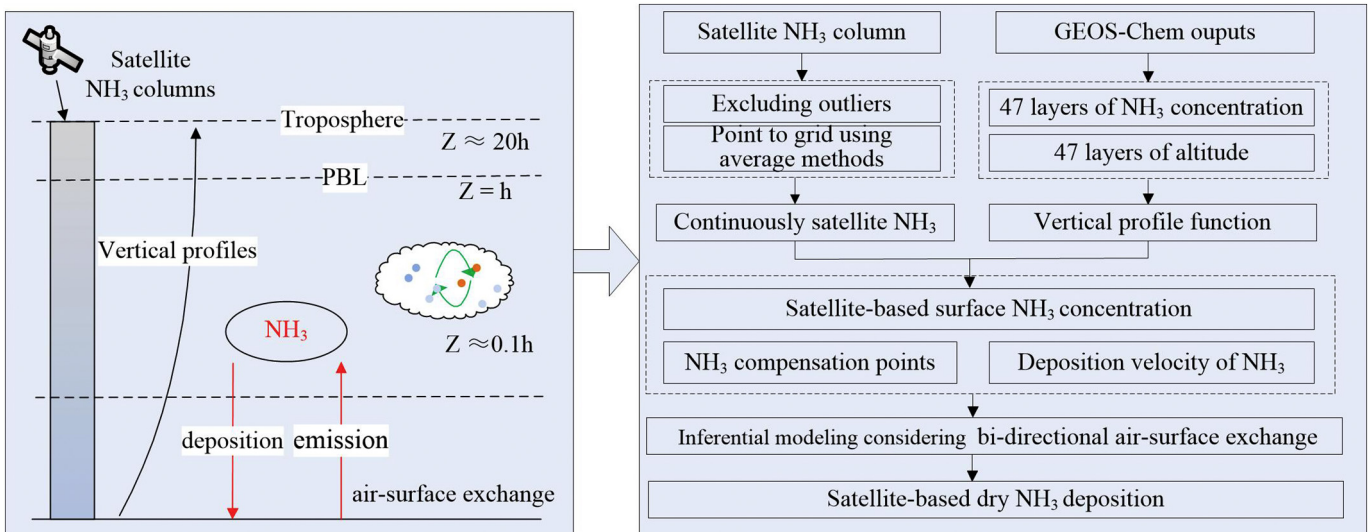

Fig. 1. Diagram and Flowchart of using satellite data to estimate dry NH_3 deposition with the bi-directional NH_3 exchange process.

we can retrieve satellite-based surface NH_3 by the following equation (Liu et al., 2019):

$$C = \frac{G_{GEOS-Chem}}{\Omega_{GEOS-Chem}} \times \Omega_{IASI}^{9-10} \times \frac{G_{GEOS-Chem}^{1-24}}{G_{GEOS-Chem}^{9-10}} \quad (5)$$

where C indicates the IASI-derived surface NH_3; $\frac{G_{GEOS-Chem}}{\Omega_{GEOS-Chem}}$ represents the ratio of surface NH_3 to NH_3 columns by GEOS-Chem; Ω_{IASI}^{9-10} indicates IASI NH_3 column at overpass time (9–10 am); $\frac{G_{GEOS-Chem}^{1-24}}{G_{GEOS-Chem}^{9-10}}$ indicates the ratio of daily average to that at 9–10 am.

When C is greater than C_0, the NH_3 flux will be downward, and when C is less than C_0, the NH_3 flux will be upward. C_o can be calculated by

$$C_0 = \left(\frac{C}{R_a + R_b} + \frac{C_{st}}{R_{st}} + \frac{C_g}{R_{ac} + R_g} \right) \left(\frac{1}{R_a + R_b} + \frac{1}{R_{st}} + \frac{1}{R_{ac} + R_g} + \frac{1}{R_{cut}} \right)^{-1} \quad (6)$$

where R_{ac}, in-canopy aerodynamic; R_g, soil; R_{cut}, cuticle; and R_{st}, stomatal resistance. C_{st} and C_g are stomatal and soil compensation points.

C_o can be calculated by setting $C = C_o$ in Eq. (6):

$$C_0 = \left[\frac{C_{st}}{R_{st}} + \frac{C_g}{R_{ac} + R_g} \right] \left[\frac{1}{R_{st}} + \frac{1}{R_{ac} + R_g} + \frac{1}{R_{cut}} \right]^{-1} \quad (7)$$

C_{st} and C_g can be both simplified by the formula:

$$\begin{cases} C_{st} = \frac{A}{T_{st}} \exp\left(-\frac{B}{T_{st}}\right) \tau_{st} & C_g = \frac{A}{T_g} \exp\left(-\frac{B}{T_g}\right) \tau_g \end{cases} \quad (8)$$

where T_{st} (T_g) is the stomata (soil) temperature; τ_{st} (τ_g) is the stomatal (soil) emission potential; A and B (fixed parameters) are 161,500 and 10,378 (Zhang et al., 2010).

$$\tau_g = \frac{[NH_4^+]_g}{[H^+]_g} \quad (9)$$

where $[NH_4^+]_g$ and $[H^+]_g$ are NH_4^+ and H^+ concentrations in the soil.

We used the DNDC model to simulate the NH_4^+ and H^+ concentration in the soil and calculated τ_g, as shown in Fig. S2. Briefly, the DNDC is a processed model, which can be used to simulate the biogeochemical processes and model the NH_4^+ and H^+ concentration in the soil, with consideration of the chemical fertilizer N, manure N as well as litter N from plant residues.

$$\tau_{st} = \frac{[NH_4^+]_{st}}{[H^+]_{st}} \quad (10)$$

where $[NH_4^+]_{st}$ and $[H^+]_{st}$ are NH_4^+ and H^+ concentrations in the apoplastic fluid. The τ_{st} was highly linked with the LAI (Zhang et al., 2010), and varied significantly by different types of land use (Wen et al., 2014; Whaley et al., 2018; Zhang et al., 2010). We referred to these studies (Wen et al., 2014; Whaley et al., 2018) by setting: If LAI < 0.5, $\tau_{st} = 0$; If LAI ≥ 0.5, $\tau_{st} = 300$, 800, 300 for forests, farmlands and grasslands, respectively.

4. Results

4.1. Global estimates of surface NH_3 concentration

Satellite-based surface NH_3 estimates during 2008–2016 have been obtained by combining IASI NH_3 columns and the NH_3 vertical profiles using Eq. (5) (Liu et al., 2019). We considered the effects of spatially dynamic NH_3 vertical profiles rather than the fixed vertical profiles to gain the surface NH_3 estimates. Overall, satellite-based NH_3 estimates

achieved a reasonably high consistency with measured surface NH_3 concentrations over the monitoring sites ($R^2 = 0.76$) (Liu et al., 2019). As illustrated in Fig. 2a, in the Northern Hemisphere, high surface NH_3 concentrations above 5 µg m^{-3} appeared in Eastern China and Northeastern India, followed by Northeastern and Southern China, Eastern US, Middle and South India, and Western Europe.

4.2. NH_3 compensation points

As described in the method section, the NH_3 compensation point is also an important variable influencing the estimation of dry NH_3 deposition. The NH_3 compensation point can be separated into two parts: the stomatal compensation point (C_{st}) and the ground compensation point (C_g). For these two key variables, the τ_{st} and τ_g (as the stomatal and soil NH_3 emission potential) are the two key parameters. Previous works (Cooter et al., 2010; Zhang et al., 2010) based on the ground-based observations found the τ_g was highest in the farmland soils due to the frequent N fertilization (such as urea and NH_4^+ contained chemicals). We calculated the τ_g using the processed model DNDC to quantify the τ_g, with the consideration of the effects of N fertilization and N litter. For the τ_{st}, the LAI shows a strong positive relationship with τ_{st} based on the ground-based measurements and the variable of LAI (by satellite retrievals) was added in the algorithm. Based on the calculated τ_{st} and τ_g, the C_{st} and C_g can be quantified using the Eq. (7), which can be found in Fig. 2c and d.

High C_{st} were high in forests and agricultural lands, such as the Southern and Northern India (>0.7 µg m^{-3}), Eastern China (>0.4 µg m^{-3}) and Africa North of Equator (>1.0 µg m^{-3}). The C_{st} in Eastern China, Northern India, Eastern US and Western Europe were on average 0.36, 0.49, 0.08 and 0.04 µg m^{-3}, respectively. On the other hand, high C_g had the highest values over agricultural soils with high N fertilization (C_g can be above 1 µg m^{-3}), while in natural ecosystems C_g had low values (<0.1 µg m^{-3}). The C_g in Eastern China, Northern India, Eastern US and Western Europe on average were 0.71, 0.75, 0.07 and 0.04 µg m^{-3}, respectively. Zhang et al. (Zhang et al., 2010) summarized a number of ground-based measurements on C_{st} and C_g. The τ_g in agricultural soils in this study was modeled using the processed model DNDC producing a C_g above 1 µg m^{-3} over high N fertilization areas, similar to the majority of ground-based measurements by Zhang et al. (Zhang et al., 2010). The τ_{st} in the forest in this study was set as 300, producing a C_{st} within 0.0–1.0 µg m^{-3}, close to the observed values from Zhang et al. (Zhang et al., 2010). The τ_{st} in agricultural land in this study was set as 800, producing a C_{st} within 0.2–2.0 µg m^{-3}, which are believed as the conservative estimates. The τ_{st} in other natural vegetative canopies in this study was set as 20, producing a C_{st} below 0.1 µg m^{-3}, which can be mostly considered as a sink of NH_3.

Regarding the seasonal variations, both C_{st} and C_g were high in warm months (May–October) and low in cold months (November–April) in the six selected regions in Northern Hemisphere (Fig. 3). Both C_{st} and C_g were highly impacted by the temperature, N availability (related to N fertilization time), and growth status (indicated by LAI). For the selected regions in Northern Hemisphere, the temperature was high from March to October, and highest in summer months (June, July and August); the N fertilization to planted crops was often applied in March to October and can lead to high NH_4^+ in the soil; for the natural ecosystems the LAI was larger in summer and spring due to more precipitation and higher temperature than those in autumn and winter. Combined with all these, the C_{st} and C_g were highest in summer (C_g can be higher than 1 µg m^{-3}), followed by spring, autumn and winter. Considering both the C_{st} and C_g, the NH_3 compensation points (Fig. 2b) can be calculated using Eq. (7). The NH_3 compensation points in ECH, NEI, EUS and WEU were on average 0.54, 0.62, 0.08 and 0.04 µg N m^{-3}, respectively, which were 11%, 17%, 5% and 3% of the averaged surface NH_3 concentration.
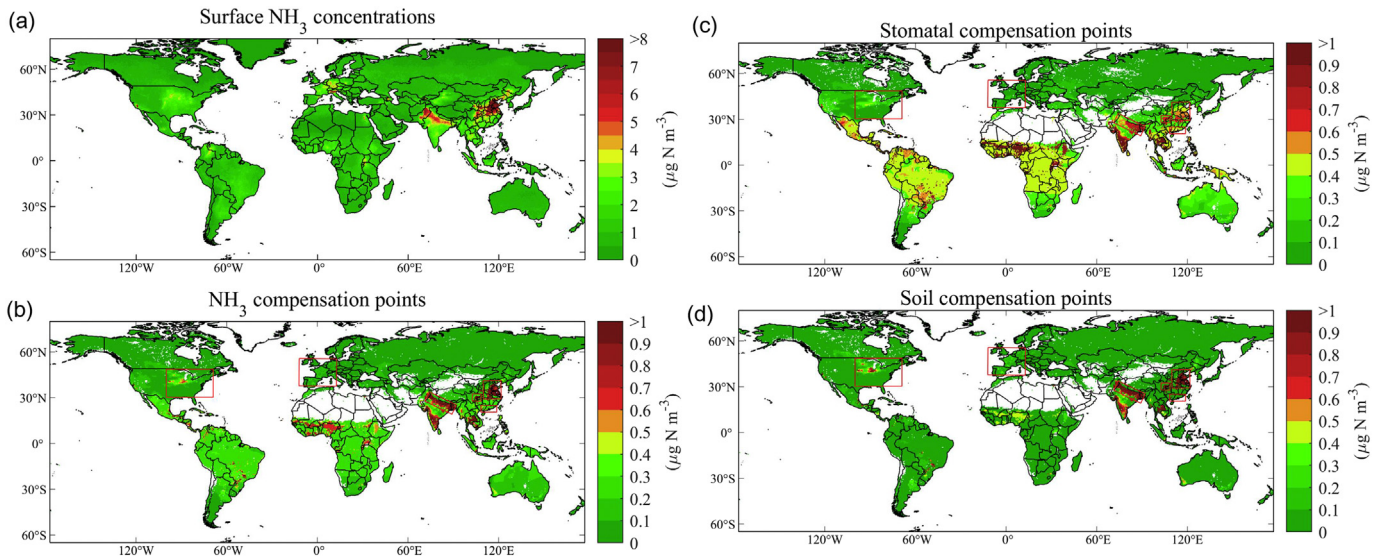
Fig. 2. Spatial maps of satellite-based surface NH_3 concentration (a), NH_3 compensation points (b), stomatal and soil compensation points (c and d) in 2014. The red rectangles include West Europe (WEU), East US (EUS), Guangdong (GD), Sichuan and Chongqing (SCH), East China (ECH), and Northeast India (NEI). The summary of surface NH_3 concentration and NH_3 compensation points in different land use types in China, US and Europe can be found in Table S1. (For interpretation of the references to colour in this figure legend, the reader is referred to the web version of this article.)

4.3. Deposition velocity of NH_3

The NH_3 V_d can be calculated by Eq. (2). The highest V_d of NH_3 (> 0.8 cm s^{-1}) occurred in the land-use type of water (Fig. 4a and b), mainly due to the adsorption of NH_3 by water (or wet climatic conditions) (Asman, 1998; Poor et al., 2001; Van der Graaf et al., 2018; Yang et al., 2010). The V_d varied between 0.12 and 1.07 cm s^{-1} in China in different land use types, and was on average 0.51, 0.52, 0.63, 0.49 and 0.37 cm s^{-1} in farmland, urban area, water, forest and grassland, respectively; In the US, the V_d varied between 0.18 and 1.03 cm s^{-1}, and was 0.52, 0.49, 0.68, 0.55 and 0.45 cm s^{-1} in farmland, urban area, water, forest and grassland, respectively; In Europe, the range of NH_3 V_d was 0.14–1.12 cm s^{-1}, and the averages were 0.54, 0.55, 0.61, 0.50 and 0.56 cm s^{-1} in farmland, urban area, water and grassland, respectively.

4.4. Dry deposition of NH_3

Combined by surface NH_3 concentrations, NH_3 compensation points and V_d, the dry NH_3 deposition can be estimated using the Eq. (1). Notably, we also applied our estimates of NH_3 compensation points to the ground-based measurements, to calculate dry NH_3 deposition at the monitoring sites. Finally, we contrasted satellite-derived estimates with the monitoring dry NH_3 deposition. Overall, satellite-based estimates were in general consistent with the ground measurements ($R^2 = 0.65$ in Fig. S4). The average estimated dry NH_3 deposition in 2014 at the monitoring sites was 3.49 kg N ha^{-1}, which was close to

the measurements at the monitoring sites (3.34 kg N ha^{-1}). Regarding different regions, the regression of IASI-derived dry NH_3 deposition with ground-based measurements over China had the highest R^2 (0.68), followed by Europe (0.52) and the US (0.43). Better accuracy for China than other regions is related to the thermal contrast and the detection limits by satellite instruments (Liu et al., 2019; Whitburn et al., 2016); China also had the largest RMSE, followed by Europe and the US. 73% of the estimates were within ±50% of observations. For China, 71% and 77% of estimates were within ±50% observations in urban and rural land; For the US and the Europe, these sites were located at rural sites (Li et al., 2016; Tørseth et al., 2012). We did not found significant difference in the validation of satellite estimates in different land use. An underestimation in the estimated dry NH_3 deposition occurred in China (4.74 vs. 7.33 kg N ha^{-1}), while a slight overestimation of dry NH_3 deposition occurred in the US (2.16 vs. 1.79 kg N ha^{-1}) and Europe (2.95 vs. 1.90 kg N ha^{-1}). This is mainly because that a number of monitoring sites in China were located in the agricultural land (had high surface concentrations), while most of the sites in Europe and the US were located in the background areas (having low surface concentrations). This suggests that these ground-based sites may be not well representative for a given grid cell as the satellite indicated. Nevertheless, the satellite-derived dry NH_3 deposition can generally reflect the spatial gradients that the ground-based measurements gained over the regions with intensively distributed monitoring sites. Generally, the hotspots of dry NH_3 deposition (Fig. 4d) mainly occurred in the farmlands (such as East China, Sichuan Basin, Northern India and East US). The global dry NH_3
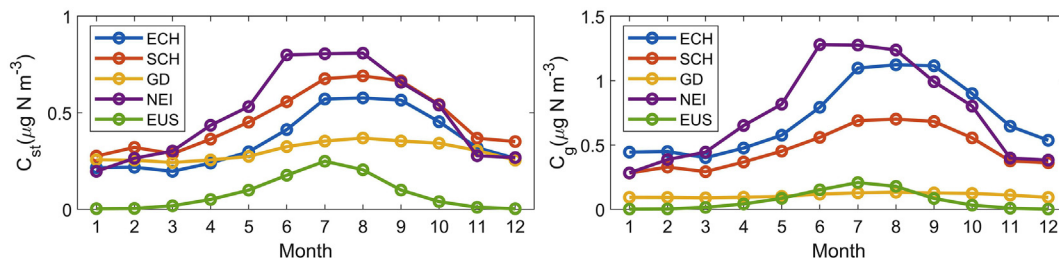

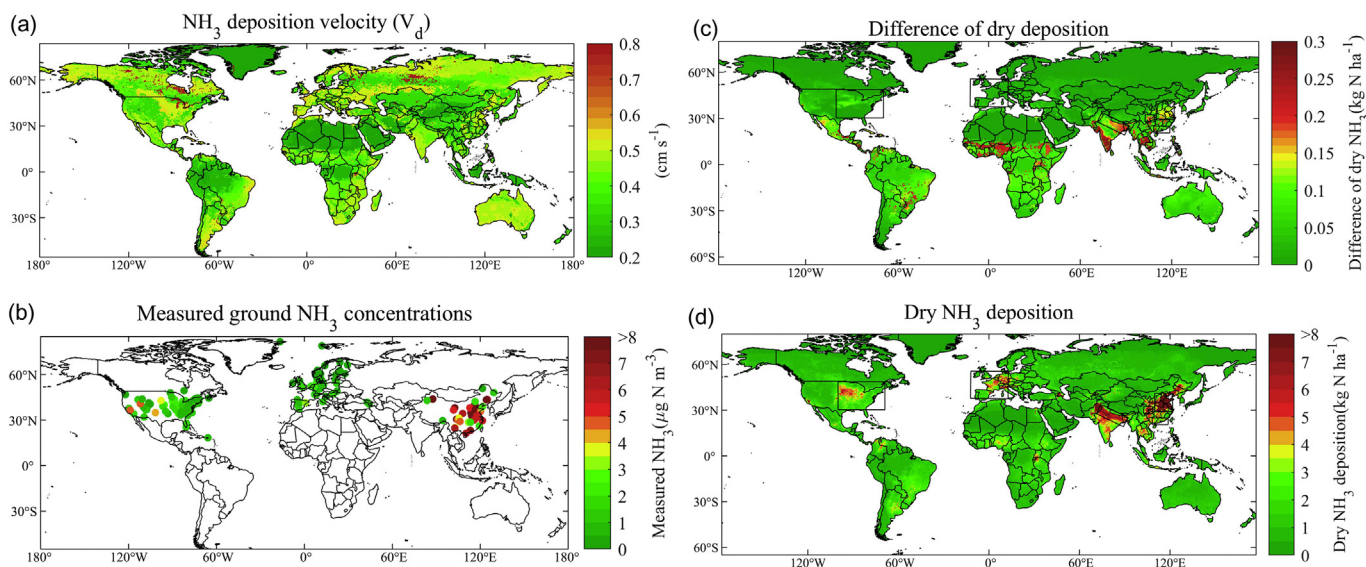**Fig. 3.** Monthly variations of C_{st} and C_g in selected regions.

Fig. 4. Spatial distribution of NH$_3$ deposition velocity (a), measured dry NH$_3$ concentration (b), spatial difference of dry NH$_3$ deposition between using the bidirectional and unidirectional NH$_3$ exchange methods (c), satellite-derived dry NH$_3$ deposition (d). The validation results between satellite estimates and ground-based measurements can be found in Fig. S4.

deposition over 8 kg N ha^{-1} appeared in East China, Pakistan, and Northern India. Dry NH$_3$ deposition at 4–8 kg N ha^{-1} occurred in Eastern, Southern, Northeastern and Southwestern China, Northern and Middle India, Vietnam, Western Europe, Eastern US.

4.5. Trends in dry deposition of NH$_3$ in six hotspot regions

We calculated annual changes of dry NH$_3$ deposition based on satellite-based estimates (Fig. 5a), and six hotspot regions with high dry NH$_3$ deposition were selected to analyze the trends (2008–2016) including ECH, SCH, GD, NEI, EUS and WEU (Fig. 5b). An annual increase of 0.27 and 0.13 kg N ha^{-1} y^{-1} in dry NH$_3$ deposition during 2008–2016 occurred in ECH ($R = 0.89$ and $p = .001$), and SCH ($R = 0.68$ and $p = .043$). The trends of dry NH$_3$ deposition during 2008–2016 in GD, EUS and WEU were not significant ($p > .05$), with small fluctuations (varying within ±0.02 kg N ha^{-1} y^{-1}). NEI was identified with a decreasing trend in dry NH$_3$ deposition (-0.09 kg N ha^{-1}, R = 0.68 and p = .043). A continuous increase of dry NH$_3$ deposition occurred in ECH and SCH, as the densely populated agricultural production areas, where NH$_3$ emissions were reported to account for 40–60% of China's total NH$_3$ emissions (Huang et al., 2012). The fertilizer use, animal husbandry and industry were believed as the main sources of NH$_3$, and fertilizer use contributed the most to NH$_3$ deposition (~50%) (Wei et al., 2019b; Xu et al., 2018). Before 2015, there were no strict policies and regulations to control NH$_3$ emissions in China, which led to the continuous growth of NH$_3$ deposition. NEI is the only selected hotspot region with a significant downward trend of NH$_3$ deposition. The significant downward trend is consistent with that of IASI NH$_3$ columns (Van Damme et al., 2015). The decline of dry NH$_3$ deposition in NEI may be related to the continuous increase of acid gases (SO$_2$ and NO$_2$) in India, which may accelerate the conversion of NH$_3$ to NH$_4^+$ (Lachatre et al., 2019; Liu et al., 2018).

5. Discussion

5.1. Differences and similarities with previous studies of estimating dry NH$_3$ deposition

Most of the previous estimates on large-scale dry NH$_3$ deposition only concerned the downward NH$_3$ process, and neglected the upward process (Jia et al., 2016; Yu et al., 2019; Zhao et al., 2017). However, the

NH$_3$ air-surface exchange is bidirectional, and the upward NH$_3$ flux cannot be ignored, especially in areas with high soil NH$_3$ emission potentials (Bouwman et al., 2002; Zhang et al., 2010). Although the bidirectional NH$_3$ exchange was observed over a number of ground measurements, most of the current atmospheric models only include the deposition process, and ignored the mechanism of bidirectional air-surface exchange of NH$_3$ (such as the widely used model GEOS-Chem). Thus, previous estimates can only represent the upper limit estimates, especially for regions with large NH$_3$ emission potentials at warm conditions (Feng et al., 2015; Li, 2000).

This study used the satellite retrievals to estimate the dry NH$_3$ deposition by bi-directional NH$_3$ exchange models at a global scale. Fig. 3 shows the monthly variations of NH$_3$ compensation points in hotspot regions. In general, high NH$_3$ compensation points occurred during warm months (April to October) in six selected regions, due to the higher temperature, N fertilization and growth status (indicated by LAI). Our results showed that the C_{st} and C_g were highest during the summer (June, July and August) and C_g could be above 1 µg m^{-3} (such as in Eastern China, Sichuan Chongqing and Northern India regions with high N fertilization), implying the importance of considering the NH$_3$ compensation points for estimating dry NH$_3$ deposition. A relatively large uncertainty existed on estimating the NH$_3$ compensation points in previous studies, which was mainly caused by the uncertainty of the parameters of τ_{st} and τ_g, which were determined empirically. We considered the management practices on τ_g including all N inputs (N fertilization, manure N and N litter), and used the processed model DNDC to model the τ_g globally. Thus, our results may provide a more realistic status of current NH$_3$ compensation points, especially in managed agricultural land type.

Overall, the global average of NH$_3$ compensation points was 0.12 µg N m^{-3}, which was about 12% of global surface NH$_3$ concentrations. This suggests an approximately 14% overestimation of dry NH$_3$ deposition using unidirectional methods. If the upward NH$_3$ flux was ignored, it will cause 11%, 17%, 5% and 3% overestimation in dry NH$_3$ deposition in Eastern China, Northern India, Eastern US and Western Europe. The estimated mean global dry NH$_3$ deposition in the land were 1.39 kg N ha^{-1}, similar to the estimates (1.44 kg N ha^{-1}) by a previous study (Jia et al., 2016), summarizing 267 monitoring sites around the globe. The validation of estimated global dry NH$_3$ deposition has shown a high predictive power of proposed satellite-based methods ($R^2 = 0.65$), although an underestimation in China and a slight
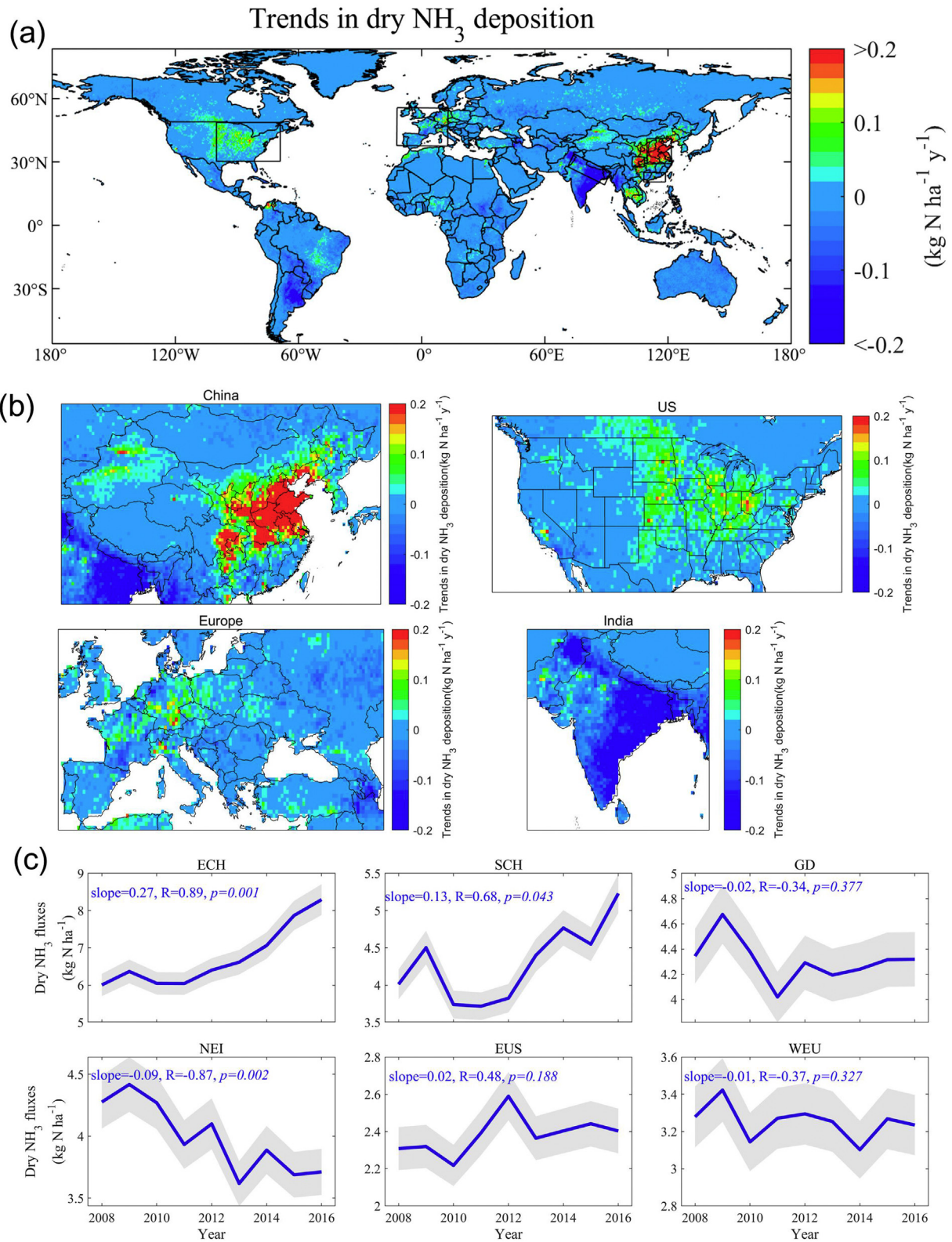
Fig. 5. Annual changes of dry NH_3 deposition globally. (a) spatial map of gridded changes of dry NH_3 deposition globally; (b) the same as (a) but focusing on China, the US, Europe and India; (c) trend of dry NH_3 deposition over six selected regions including ECH, SCH, GD, NEI, EUS and WEU.

overestimation in the US and Europe still exist. This inconsistency may be due to the limited spatial representatives of the monitoring sites at a given satellite grid (0.25°) as well as the uncertainty in the satellite-based estimates.

5.2. Prospects for estimating surface NH_3 concentrations

This study established a satellite-based approach for deriving surface NH_3 estimates. In this study, we gave a brief description of the validation

results, and more detailed information has been demonstrated in the previous paper (Liu et al., 2019). Our previous study (Liu et al., 2019) focused on the approach of estimating surface NH_3 concentrations, while this study aims to develop satellite-based methods for estimating dry NH_3 deposition considering the bidirectional NH_3 air-surface exchange. Although we found better accuracy in the satellite estimates of surface NH_3 concentrations than the GEOS-Chem modeling surface NH_3 concentrations, challenges still exist for generating higher spatial resolutions of surface NH_3 concentrations. First, the accuracy of satellite estimates can be also determined by the thermal contrast (TC) and the detection limits of the satellite instruments. The accuracy increases with increasing atmospheric NH_3 abundance and TC. However, for low TC and NH_3 abundance, the uncertainty of satellite NH_3 retrievals can be high. Second, IASI-derived NH_3 concentrations are instantaneous values around 9:30 a.m., and may not representative of the daily average of NH_3 concentrations. We employed the ratio (the daily average of NH_3 concentration to that at 9–10 am) to convert the instantaneous values to daily average NH_3 concentrations. However, this may cause large uncertainties because the GEOS-Chem may not well reconstruct this relationship. We have no hourly measured NH_3 concentrations in a day, and cannot test the validity of the conversion of the instantaneous values to daily average NH_3 concentrations using the GEOS-Chem. Third, the estimated global surface NH_3 concentration can be considered to be conservative values, rather than overestimated values since the surface concentration are the values at about 50–60 m above the ground (the middle altitude in the bottom layer by GEOS-Chem). In reality, most of the monitoring sites focusing on the surface NH_3 concentrations were often set at the height of 1–50 m (lower than the height we estimated), and higher NH_3 concentrations often occurred at the lower height compared with those at a higher height. Fourth, this study assumes the relationship between surface NH_3 concentrations and NH_3 columns are scale independent. In other words, the relationship (NH_3 vertical profiles) gained at the coarse resolution from GEOS-Chem was directly used to the IASI's fine resolution without corrections. This scale effect, however, may be significant when the resolution is finer than 0.1º (lower than the actual resolutions that IASI can capture).

5.3. Prospects for estimating NH_3 compensation points

The C_{st} and C_g are acknowledged as the key variables to determine the NH_3 compensation points. The τ_{st} and τ_g were the key parameters for quantifying the C_{st} and C_g. For the first time, this study used the processed model DNDC to simulate the τ_g, and numerously studies have shown much higher τ_g in fertilized soils than the natural ecosystem soils. We considered the effects of N fertilizer on modeling τ_g, and provided more details of spatial gradients globally. Thus this study should be more reasonable than previous studies only using the fixed τ_g values in each land type. But, for the τ_{st}, we adopted the methods of a previous study (Zhang et al., 2010), and added the LAI (having significant effects on τ_{st}) into our algorithms. We set: If LAI < 0.5, τ_{st}=0; If LAI ≥0.5, τ_{st}= 300, 800, 300 for forests, farmlands and grasslands, respectively. The τ_{st} values for different land types used in this study were based on the ground-based measurements that can be considered as conservative estimates. To date, the NH_4^+ and H^+ concentrations in the apoplastic fluid can be hardly modeled on a global scale. The mechanism of determining the NH_4^+ and H^+ concentrations in the apoplastic fluid at large scales should be studied further.

6. Conclusions

It is important to estimate large-scale dry NH_3 deposition, with potentially detrimental impacts on ecosystems. This work provides satellite-based estimates of dry NH_3 deposition at a global scale, taking into account of the bi-directional NH_3 exchange during 2008–2016. High NH_3 compensation points occurred during warm months (April to October) in the selected hotspot regions, and were above 1 µg m^{-3}

during the summer months in China and India. We found 11%, 17%, 5% and 3% overestimations in dry NH_3 deposition in Eastern China, Northern India, Eastern US and Western Europe, respectively, when ignoring the upward NH_3 process for estimating dry deposition. IASI-derived estimates generally matched with measured dry NH_3 deposition over monitoring sites ($R^2 = 0.65$). Global dry NH_3 deposition over 8 kg N ha^{-1} was mainly distributed in the Eastern China, Northern and Central Pakistan, and Northern India. An annual increase rate of 0.27 and 0.13 kg N ha^{-1} y^{-1} in dry NH_3 deposition during 2008–2016 occurred in East China and Sichuan Basin, which are the major Chinese agricultural regions. The satellite-derived dry NH_3 deposition can be used to represent the current status of dry NH_3 deposition, considering the possible NH_3 bidirectional exchange, at a global scale, and can provide valuable datasets for evaluating the impact of N contamination on soil, water, climate and biogeochemical cycles.

CRediT authorship contribution statement

Lei Liu: Conceptualization, Methodology, Writing - original draft. **Xiuying Zhang:**Writing - review & editing.**Wen Xu:**Writing - review & editing.**Xuejun Liu:**Writing - review & editing.**Jing Wei:**Writing - review & editing.**Zhen Wang:**Validation, Formal analysis, Visualization, Investigation.**Yuyu Yang:**Validation, Formal analysis, Visualization, Investigation.

Declaration of competing interest

The authors declare that they have no known competing financial interests or personal relationships that could have appeared to influence the work reported in this paper.

Acknowledgements

Appendix A. Supplementary data

Supplementary data to this article can be found online at https://doi.org/10.1016/j.scitotenv.2020.139189.

References

Asman, W.A.H., 1998. Factors influencing local dry deposition of gases with special reference to ammonia. Atmos. Environ. 32, 415–421.

Azouz, N., Drouet, J.L., Beekmann, M., Siour, G., Kruit, R.W., Cellier, P., 2019. Comparison of spatial patterns of ammonia concentration and dry deposition flux between a regional Eulerian chemistry-transport model and a local Gaussian plume model. Air Quality, Atmosphere & Health 1–11.

Bobrutzki, K.V., Braban, C.F., Famulari, D., Jones, S.K., Blackall, T., Smith, T.E.L., et al., 2010. Field inter-comparison of eleven atmospheric ammonia measurement techniques. Atmospheric Measurement Techniques 2, 91–112 3,(2010-01-27).

Bouwman, A.F., Boumans, L.J.M., Batjes, N.H., 2002. Estimation of global NH_3 volatilization loss from synthetic fertilizers and animal manure applied to arable lands and grasslands. Glob. Biogeochem. Cycles 16, 1–11.

Chen, D., Wang, Y., Mcelroy, M.B., He, K., 2009. Regional CO pollution in China simulated by the high-resolution nested-grid GEOS-Chem model. Atmos. Chem. Phys. 9, 5853–5887.

Cooter, E.J., Bash, J.O., Walker, J.T., Jones, M.R., Robarge, W., 2010. Estimation of NH3 bi-directional flux from managed agricultural soils. Atmos. Environ. 44, 2107–2115.

Endo, T., Yagoh, H., Sato, K., Matsuda, K., Hayashi, K., Noguchi, I., et al., 2011. Regional characteristics of dry deposition of sulfur and nitrogen compounds at EANET sites in Japan from 2003 to 2008. Atmos. Environ. 45, 1259–1267.

Erisman, J.W., Van Pul, A., Wyers, P., 1994. Parametrization of surface resistance for the quantification of atmospheric deposition of acidifying pollutants and ozone. Atmos. Environ. 28, 2595–2607.

Feng, Z., Ciais, P., Hayashi, K., Galloway, J., Kim, D.G., Yang, C., et al., 2015. Re-estimating NH_3 emissions from Chinese cropland by a new nonlinear model. Environ. Sci. Technol. 50, 564–572.

Fountoukis, C., Nenes, A., 2007. ISORROPIA II: a computationally efficient thermodynamic equilibrium model for aerosols. Atmos. Chem. Phys. 7, 4639–4659.

Galloway, J.N., Townsend, A.R., Erisman, J.W., Bekunda, M., Cai, Z., Freney, J.R., et al., 2008. Transformation of the nitrogen cycle: recent trends, questions, and potential solutions. Science 320, 889–892.

Graaf, Scvd, Dammers, E., Schaap, M., Erisman, J.W., 2018. How are NH_3 dry deposition estimates affected by combining the LOTOS-EUROS model with IASI-NH3 satellite observations? Atmos. Chem. Phys. 18, 13173–13196.

Huang, X., Song, Y., Li, M., Li, J., Huo, Q., Cai, X., et al., 2012. A high resolution ammonia emission inventory in China. Glob. Biogeochem. Cycles 26, 1–14.

Husted, S., Mattsson, M., Schjoerring, J.K., 2010. Ammonia compensation points in two cultivars of Hordeum vulgare L. during vegetative and generative growth. Plant Cell Environ. 19, 1299–1306.

Jia, Y., Yu, G., Gao, Y., He, N., Wang, Q., Jiao, C., et al., 2016. Global inorganic nitrogen dry deposition inferred from ground-and space-based measurements. Sci. Rep. 6, 1–11.

Kharol, S.K., Shephard, M.W., McLinden, C.A., Zhang, L., Sioris, C.E., O'Brien, J.M., et al., 2018. Dry deposition of reactive nitrogen from satellite observations of Ammonia and nitrogen dioxide over North America. Geophys. Res. Lett. 45, 1157–1166.

Lachatre, M., Fortems-Cheiney, A., Foret, G., Siour, G., Dufour, G., Clarisse, L., et al., 2019. The unintended consequence of SO_2 and NO_2 regulations over China: increase of ammonia levels and impact on PM2.5 concentrations. Atmos. Chem. Phys. 19, 6701–6716.

Li, C.S., 2000. Modeling trace gas emissions from agricultural ecosystems. In: Wassmann, R., Lantin, R.S., Neue, H.-U. (Eds.), Methane Emissions from Major Rice Ecosystems in Asia. Springer Netherlands, Dordrecht, pp. 259–276.

Li, Y., Schichtel, B.A., Walker, J.T., Schwede, D.B., Chen, X., Lehmann, C.M., et al., 2016. Increasing importance of deposition of reduced nitrogen in the United States. Proc. Natl. Acad. Sci. 113, 5874–5879.

Liu, L., Zhang, X., Xu, W., Liu, X., Li, Y., Lu, X., et al., 2017. Temporal characteristics of atmospheric ammonia and nitrogen dioxide over China based on emission data, satellite observations and atmospheric transport modeling since 1980. Atmospheric Chemistry & Physics 17, 1–32.

Liu, M., Huang, X., Song, Y., Xu, T., Wang, S., Wu, Z., et al., 2018. Rapid SO_2 emission reductions significantly increase tropospheric ammonia concentrations over the North China plain. Atmos. Chem. Phys. 18, 17933–17943.

Liu, L., Zhang, X., Wong, A.Y.H., Xu, W., Liu, X., Li, Y., et al., 2019. Estimating global surface ammonia concentrations inferred from satellite retrievals. Atmos. Chem. Phys. 19, 12051–12066.

Ludwig, J., Meixner, F.X., Vogel, B., Förstner, J., 2001. Soil-air exchange of nitric oxide: an overview of processes, environmental factors, and modeling studies. Biogeochemistry 52, 225–257.

Nemitz, E., Sutton, M.A., Schjoerring, J.K., Husted, S., Paul Wyers, G., 2000. Resistance modelling of ammonia exchange over oilseed rape. Agric. For. Meteorol. 105, 405–425.

Nemitz, E., Flynn, M., Williams, P.I., Milford, C., Theobald, M.R., Blatter, A., et al., 2001. A relaxed Eddy accumulation system for the automated measurement of atmospheric Ammonia fluxes. Water, Air and Soil Pollution: Focus 1, 189–202.

Poor, N., Pribble, R., Greening, H., 2001. Direct wet and dry deposition of ammonia, nitric acid, ammonium and nitrate to the Tampa Bay estuary, FL, USA. Atmos. Environ. 35, 3947–3955.

Pye, H.O.T., Liao, H., Wu, S., Mickley, L.J., Jacob, D.J., Henze, D.K., et al., 2009. Effect of changes in climate and emissions on future sulfate-nitrate-ammonium aerosol levels in the United States. Journal of Geophysical Research: Atmospheres 114.

Qi, J.H., Shi, J.H., Gao, H.W., Sun, Z., 2013. Atmospheric dry and wet deposition of nitrogen species and its implication for primary productivity in coastal region of the Yellow Sea, China. Atmos. Environ. 81, 600–608.

Reay, D.S., Dentener, F., Smith, P., Grace, J., Feely, R.A., 2008. Global nitrogen deposition and carbon sinks. Nat. Geosci. 1, 430–437.

Sickles II, J.E., Shadwick, D.S., 2015. Air quality and atmospheric deposition in the eastern US: 20 years of change. Atmos. Chem. Phys. 15, 173–197.

Sutton, M.A., Asman, W.A.H., Schøring, J.K., 1994. Dry deposition of reduced nitrogen. Tellus Series B-chemical & Physical Meteorology 46, 255–273.

Sutton, M.A., Burkhardt, J.K., Guerin, D., Nemitz, E., Fowler, D., 1998. Development of resistance models to describe measurements of bi-directional ammonia surface–atmosphere exchange. Atmos. Environ. 32, 473–480.

Sutton, M.A., Dragosits, U., Tang, Y.S., Fowler, D., 2000. Ammonia emissions from non-agricultural sources in the UK - source testing results. Atmos. Environ. 34, 855–869.

Sutton, M.A., Tang, Y.S., Miners, B., Fowler, D., 2001. A new diffusion denuder system for long-term, regional monitoring of atmospheric Ammonia and ammonium. Water Air & Soil Pollution Focus 1, 145–156.

Sutton, M.A., Flower, D., Moncriefe, J.B., 2010. The exchange of atmospheric ammonia with vegetated surfaces. I: unfertilized vegetation. Q. J. R. Meteorol. Soc. 119, 1023–1045.

Sutton, M.A., Reis, S., Riddick, S.N., Dragosits, U., Nemitz, E., Theobald, M.R., et al., 2013. Towards a climate-dependent paradigm of ammonia emission and deposition. Philos. Trans. R. Soc. Lond. B Biol. Sci. 368.

Tørseth, K., Aas, W., Breivik, K., Fjæraa, A.M., Fiebig, M., Hjellbrekke, A.G., et al., 2012. Introduction to the European monitoring and evaluation Programme (EMEP) and observed atmospheric composition change during 1972–2009. Atmos. Chem. Phys. 12, 5447–5481.

Van Damme, M., Clarisse, L., Dammers, E., Liu, X., Nowak, J., Clerbaux, C., et al., 2014a. Towards validation of ammonia (NH_3) measurements from the IASI satellite. Atmospheric Measurement Techniques 7, 12125–12172.

Van Damme, M., Wichink Kruit, R., Schaap, M., Clarisse, L., Clerbaux, C., Coheur, P.F., et al., 2014b. Evaluating 4 years of atmospheric ammonia (NH_3) over Europe using IASI satellite observations and LOTOS-EUROS model results. J. Geophys. Res.-Atmos. 119, 9549–9566.

Van Damme, M., Erisman, J.W., Clarisse, L., Dammers, E., Whitburn, S., Clerbaux, C., et al., 2015. Worldwide spatiotemporal atmospheric ammonia (NH_3) columns variability revealed by satellite. Geophys. Res. Lett. 42, 8660–8668.

Van Damme, M., Whitburn, S., Clarisse, L., Clerbaux, C., Hurtmans, D., Coheur, P.F., 2017. Version2 of the IASI NH_3 neural network retrieval algorithm: near-real-time and reanalysed datasets. Atmos. Meas. Tech. 10, 1–14.

Van Damme, M., Clarisse, L., Whitburn, S., Hadji-Lazaro, J., Hurtmans, D., Clerbaux, C., et al., 2018. Industrial and agricultural ammonia point sources exposed. Nature 564, 99–103.

Van der Graaf, S.C., Dammers, E., Schaap, M., Erisman, J.W., 2018. Technical note: how are NH_3 dry deposition estimates affected by combining the LOTOS-EUROS model with IASI-NH_3 satellite observations? Atmos. Chem. Phys. 18, 13173–13196.

Wang, Y., Logan, J.A., Jacob, D.J., 1998. Global simulation of tropospheric O 3 -NO x -hydrocarbon chemistry: 2. Model evaluation and global ozone budget. Journal of Geophysical Research Atmospheres 103, 10727–10755.

Warner, J.X., Wei, Z., Strow, L.L., Dickerson, R.R., Nowak, J.B., 2016. The global tropospheric ammonia distribution as seen in the 13-year AIRS measurement record. Atmos. Chem. Phys. 16, 5467–5479.

Wei, J., Huang, W., Li, Z., Xue, W., Peng, Y., Sun, L., et al., 2019a. Estimating 1-km-resolution PM2.5 concentrations across China using the space-time random forest approach. Remote Sens. Environ. 231, 111221.

Wei, J., Li, Z., Guo, J., Sun, L., Huang, W., Xue, W., et al., 2019b. Satellite-derived 1-km-resolution PM1 concentrations from 2014 to 2018 across China. Environ. Sci. Technol. 53, 13265–13274.

Wen, D., Zhang, L., Lin, J.C., Vet, R., Moran, M.D., 2014. An evaluation of ambient ammonia concentrations over southern Ontario simulated with different dry deposition schemes within STILT-Chem v0.8. Geosci. Model Dev. 7, 1037–1050.

Wesely, M., 1989. Parameterization of surface resistances to gaseous dry deposition in regional-scale numerical models. Atmos. Environ. 23, 1293–1304.

Whaley, C., Makar, P.A., Shephard, M.W., Zhang, L., Zhang, J., Zheng, Q., et al., 2018. Contributions of natural and anthropogenic sources to ambient ammonia in the Athabasca Oil Sands and North-Western Canada. Atmospheric Chemistry & Physics 18, 1–38.

Whitburn, S., Van Damme, M., Clarisse, L., Bauduin, S., Heald, C.L., Hadji-Lazaro, J., et al., 2016. A flexible and robust neural network IASI-NH3 retrieval algorithm. Journal of Geophysical Research: Atmospheres 121, 6581–6599.

Xu, W., Luo, X.S., Pan, Y.P., Zhang, L., Tang, A.H., Shen, J.L., et al., 2015. Quantifying atmospheric nitrogen deposition through a nationwide monitoring network across China. Atmos. Chem. Phys. 15, 12345–12360.

Xu, W., Liu, L., Cheng, M., Zhao, Y., Zhang, L., Pan, Y., et al., 2018. Spatial-temporal patterns of inorganic nitrogen air concentrations and deposition in eastern China. Atmos. Chem. Phys. 18, 10931–10954.

Yang, R., Hayashi, K., Zhu, B., Li, F., Yan, X., 2010. Atmospheric NH_3 and NO_2 concentration and nitrogen deposition in an agricultural catchment of eastern China. Sci. Total Environ. 408, 4624–4632.

Yu, F., Nair, A.A., Luo, G., 2018. Long-term trend of gaseous Ammonia over the United States: modeling and comparison with observations. Journal of Geophysical Research: Atmospheres 123, 8315–8325.

Yu, G., Jia, Y., He, N., Zhu, J., Chen, Z., Wang, Q., et al., 2019. Stabilization of atmospheric nitrogen deposition in China over the past decade. Nat. Geosci. 12, 424–429.

Zhang, L., Brook, J.R., Vet, R., 2003. A revised parameterization for gaseous dry deposition in air-quality models. Atmos. Chem. Phys. 3, 2067–2082.

Zhang, L., Wright, L.P., Asman, W.A.H., 2010. Bi-directional air-surface exchange of atmospheric ammonia: a review of measurements and a development of a big-leaf model for applications in regional-scale air-quality models. J. Geophy. Res-Atmos. 115, 898–907.

Zhang, R., Jing, J., Tao, J., Hsu, S.C., 2013. Chemical characterization and source apportionment of PM2.5 in Beijing: seasonal perspective. Atmos. Chem. Phys. 13, 7053–7074.

Zhao, Y., Zhang, L., Chen, Y., Liu, X., Xu, W., Pan, Y., et al., 2017. Atmospheric nitrogen deposition to China: a model analysis on nitrogen budget and critical load exceedance. Atmos. Environ. 153, 32–40.